# Probing photoionization dynamics in acetylene with angle resolved attosecond interferometry

Alexie Boyer, Vincent Loriot, Saikat Nandi, Franck Lépine

# Probing photoionization dynamics in acetylene with angle resolved attosecond interferometry

Alexie Boyer, Vincent Loriot, Saikat Nandi,* and Franck Lépine*

*Université de Lyon, Université Claude Bernard Lyon 1, CNRS, Institut Lumière Matière, F-69622 Villeurbanne, France*

E-mail: saikat.nandi@univ-lyon1.fr; franck.lepine@univ-lyon1.fr

**Abstract**

Photoionization of acetylene by extreme-ultraviolet light results in a stand-alone contribution from the outermost valence orbital followed by well-separated photoelectron bands from deeper molecular orbitals. This makes acetylene an ideal candidate for probing the photoionization dynamics in polyatomic molecules free from the spectral congestion often arising after interaction with an attosecond pulse train. Here, using an angle resolved attosecond interferometric technique we extract the photoionization time-delays for the outermost valence orbital in acetylene relative to an atomic target, namely argon. Compared to argon, the photoemission from the acetylene molecule is found to be advanced by almost 28 attoseconds. The strong variation of the relative photoionization time-delays as a function of the photoemission angle was interpreted using an analytical model based on semi-classical approximations, to be the interplay between different short-range potentials along and perpendicular to the molecular axis. Our results highlight the importance using attosecond time-resolved measurements to probe the non-spherical nature of the molecular potential, even in the case of relatively small, linear systems.

# Introduction

With its first experimental realization in 2010,[1] photoionization time-delays in ultrafast light-matter interaction have now become an indispensable tool in studying the photoionization dynamics in various systems, ranging from atoms[2,3] and molecules[4–7] in gas phase to solids[8,9] and liquids.[10] The measured photoionization time-delays were found to be sensitive towards a variety of physical properties such as Fano resonance,[11,12] shape resonance,[13–16] chirality,[17] collective excitation,[18] effect of the chemical environment,[19,20] shape[21] and symmetry[22] of the system, and mass of the target,[23,24] just to name a few. One of the interferometric techniques giving access to these time-delays is known as the Reconstruction of Attosecond Beating By Interference of Two-photon Transitions, or, RABBITT.[25] Despite being a well-

developed method, it is still challenging to implement it especially for molecular systems, since ionization by an attosecond pulse train (APT) representing a harmonic comb in the frequency domain can lead to spectral congestion in the measured photoelectron spectra.[26] Nevertheless, the RABBITT technique is now getting applied to more and more complex molecular systems, such as clusters,[21] poly-cyclic aromatic hydrocarbons[22] etc. to understand the physical origin of time-delays following ionization by an extreme ultraviolet (XUV) pulse. Here, we consider a relatively simpler system, namely acetylene ($C_2H_2$) to showcase the practicality of the RABBITT method towards probing the nature of the molecular potential. Being a linear hydrocarbon, the spectroscopic properties of acetylene are well-studied in the frequency domain using high-resolution photons from synchrotron radiation sources.[27,28] Of particular interests are the Rydberg excitation, $1\pi_u \rightarrow k\pi_g$ close to the ionization threshold and how the subsequent autoionization affects the vibrational structure observed in the ground cationic state $X\ ^2\Pi_u$ in acetylene.[29,30] Considerable attention was paid to understand whether these autoionization processes also interact with an ionization background enhanced via $\sigma_u$ shape resonance. As shown in the case of iso-electronic (to acetylene) $N_2$-molecule, existence of shape resonance in the ionization continuum usually means temporary trapping of the outgoing electron by a quasi-bound state, leading to enhancement in the photoionization time-delay.[14] Similar attosecond interferometric measurements performed in polyatomic molecules confirmed the trend.[13,15] While for ionization continuum containing different singularities, such as autoionization and shape resonances, one can expect dramatic effects in the associated time-delays, the question remains whether it is possible to extract useful information about the molecular photoionization dynamics for transition to a flat-continuum using similar techniques. Here, we address this issue by probing the ionization continuum in acetylene far away from the threshold region. In the absence of any autoionization or shape resonance, one might expect the molecular time-delay to be similar to that of an atomic target. Our angle-dependent measurements reveal that even for ionization to a flat-continuum the time-delays can be significantly altered by how the photoelectron is emitted. By taking

into account the interaction potential between the emitted photoelectron and the delocalized positively charged hole in the residual molecular ion, we could qualitatively argue that even for a simple system such as acetylene, the short-range potentials are drastically different along and perpendicular to the symmetry axis of the molecule, thus affecting the measured time-delays.

The manuscript is divided in the following sections: first, we describe in detail the experimental methodology of obtaining the time-delays for acetylene (Experimental Methods), followed by a generalized procedure to extract the ionization delays relative to an atomic target, in this case argon, and how we can interpret the observed results in terms of the variation in short range potential of the molecular cation (Results and Discussion). We conclude by providing some perspectives how similar studies can be conducted in other molecular systems that can lead to a better understanding of the photoionization dynamics.

# Experimental methods

The experiment was carried out at the Circé attosecond beamline at the Institut Lumière Matière in Lyon.[31,32] It consists of a commercially available, CEP-stable Ti:Sapphire laser system (Coherent Legend) providing near-infrared (NIR) pulses with duration of 25 fs, and energy of 2 mJ at 5 kHz repetition rate. The wavelength is centered around 800 nm. The output of this laser system is divided into two parts using a 50 : 50 beam-splitter, along the two arms of an actively stabilized Mach-Zehnder interferometer. In one arm the NIR pulse is converted into an APT using high-order harmonic generation (HHG) in xenon gas. Afterwards, the co-propagating NIR pulse was filtered out using a Sn-filter, leaving us with only three high-order harmonics: 11, 13 and 15, which were focused into the interaction region of a velocity map imaging (VMI) spectrometer using a toroidal mirror. The NIR pulse in the other arm of the interferometer was combined colinearly with the APT via a drilled mirror. It acts as the dressing field for the emitted photoelectrons in the continuum.

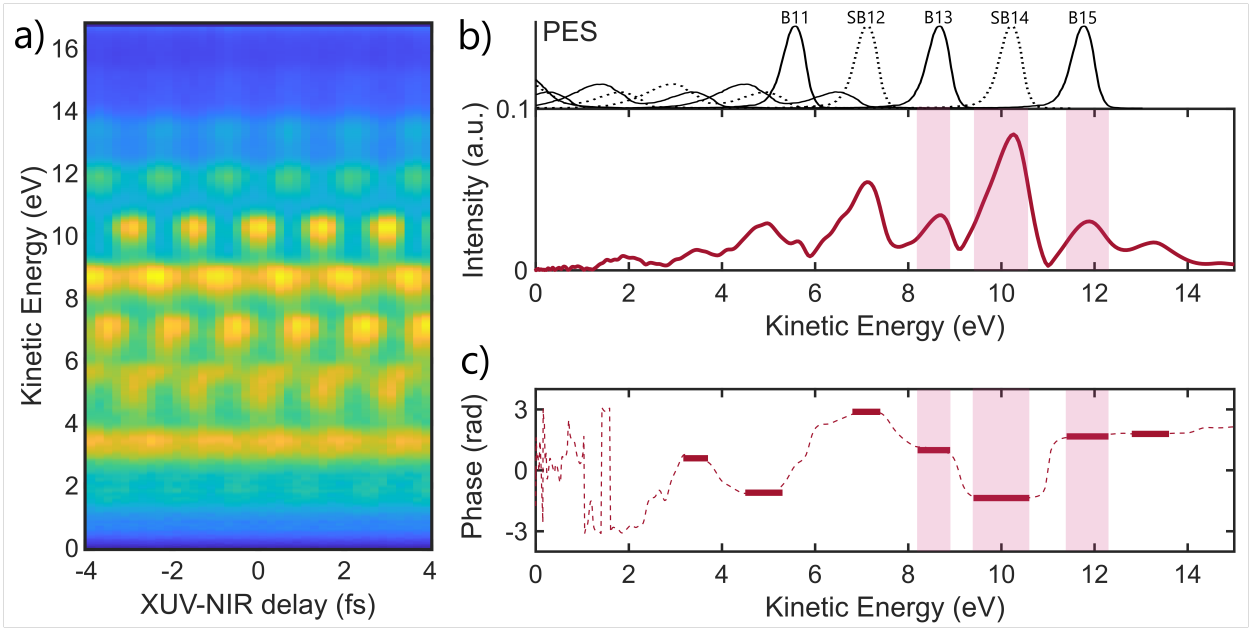


Figure 1: (a) RABBITT spectrogram for acetylene measured with an XUV harmonic comb containing three high-order harmonics: HH11, HH13 and HH15 and an NIR dressing field with intensity of 2.7 TW/cm$^2$. (b) The amplitude of oscillations at $2\omega_0$ extracted from the RABBIT map. The high-resolution photoelectron spectra obtained from synchrotron measurements[27] are attached on the top panel for identification of different main-bands (B) and sidebands (SB) in it. (c) The phase of oscillations at $2\omega_0$. In both panels (b) and (c), the three shaded areas denote B13, SB14 and B15 (from left to right).

The delay between the two pulses, XUV-APT and NIR, were varied between $-4$ fs to $+4$ fs at a step size of 200 as, using a refractive delay stage. The temporal jitter of the interferometer was estimated to be lower than 80 as. The measurements were repeated several times with different intensities of the dressing NIR field, varied using a combination of a waveplate and a polarizer, between 1.2 and 3.5 TW/cm$^2$.

The XUV-APT represents a comb of odd-order harmonic in the frequency domain. This leads to generation of main bands in the photoelectron spectra corresponding to each harmonic. In the presence of a NIR dressing field, a photoelectron emitted via one harmonic (e.g., HH13) can absorb an NIR photon while still in the continuum. Similarly, another photoelectron ejected via the adjacent higher order harmonic (e.g., HH15) can undergo a stimulated emission of a NIR photon reaching the same kinetic energy as the previous path. These two quantum pathways can interfere with each other leading to the sideband (in the

present case SB14) between the two main bands, whose amplitude oscillates as a function of the delay, $t$, between the two pulses. It constitutes the essential idea behind the RABBITT protocol.[25] The time dependent sideband amplitude can therefore be expressed as, $A_{\mathrm{SB}} = a + b\,\cos(2\omega_0 t - \phi)$, where $a$ and $b$ are constants with appropriate dimensions, and $\pi/\omega_0 = 1.33$ fs is half the optical period of the NIR laser pulse. The phase $\phi$ contains the information about the photoionization dynamics.

The angle-integrated RABBITT spectrogram for acetylene at an approximate NIR intensity of 2.7 TW/cm$^2$ is shown in Fig. 1(a). The Abel-inverted VMI spectra were integrated over an angular range of $\pm 45^\circ$ to improve the statistics. The extracted amplitude and phase of the oscillations at $2\omega_0$ in our experiment are shown in Fig. 1(b) and 1(c), respectively. The use of only three high-order harmonics significantly reduced the spectral congestion, otherwise expected in case of higher number of harmonics. In order to assign the oscillations to a particular valence band, the photoelectron spectra of acetylene measured using synchrotron radiation is displayed at the top panel of the Fig. 1(b). The electronic configuration for acetylene, excluding the C-1s electrons, can be expressed as $2\sigma_g^2\ 2\sigma_u^2\ 3\sigma_g^2\ 1\pi_u^4$, assuming $D_{\infty h}$ symmetry.[27] Using high-resolution spectroscopic data from synchrotron measurements, the binding energy regions encompassing different cationic states can be summarized as follows: $X\ ^2\Pi_u$ between $10.8-12.6$ eV, $A\ ^2\Sigma_g^+$ between $16.1-18.1$ eV and $B\ ^2\Sigma_u^+$ between $18.1-20.8$ eV.[27] Additional higher-lying cationic states, such as $C\ ^2\Sigma_g^+$, were not accessible with the harmonic comb used in our experiment. As can be understood, for lower kinetic energy electrons, especially below 6 eV, the contributions from different electronic states following ionization by different harmonics can overlap with each other leading to the loss of contrast for the attosecond oscillation in the RABBITT map. However, for kinetic energies higher than 8 eV, the photoelectrons mainly correspond to the $X$-state in the cation following ionization of the highest occupied molecular orbital (i.e., $1\pi_u$) in the neutral acetylene by harmonic order 13 and 15. The contributions corresponding to the main-band 13 and 15 as well as SB14 are highlighted in red. It can clearly be observed that the photoelectrons in

SB14 corresponds to the $X$-state only. In the following, we discuss how the measurement of the RABBITT-phase $\phi$ for SB14 for acetylene and the subsequent comparison with that of the argon atom allows us to study the underlying features of the ionization continuum of the molecule itself.

## Data analysis

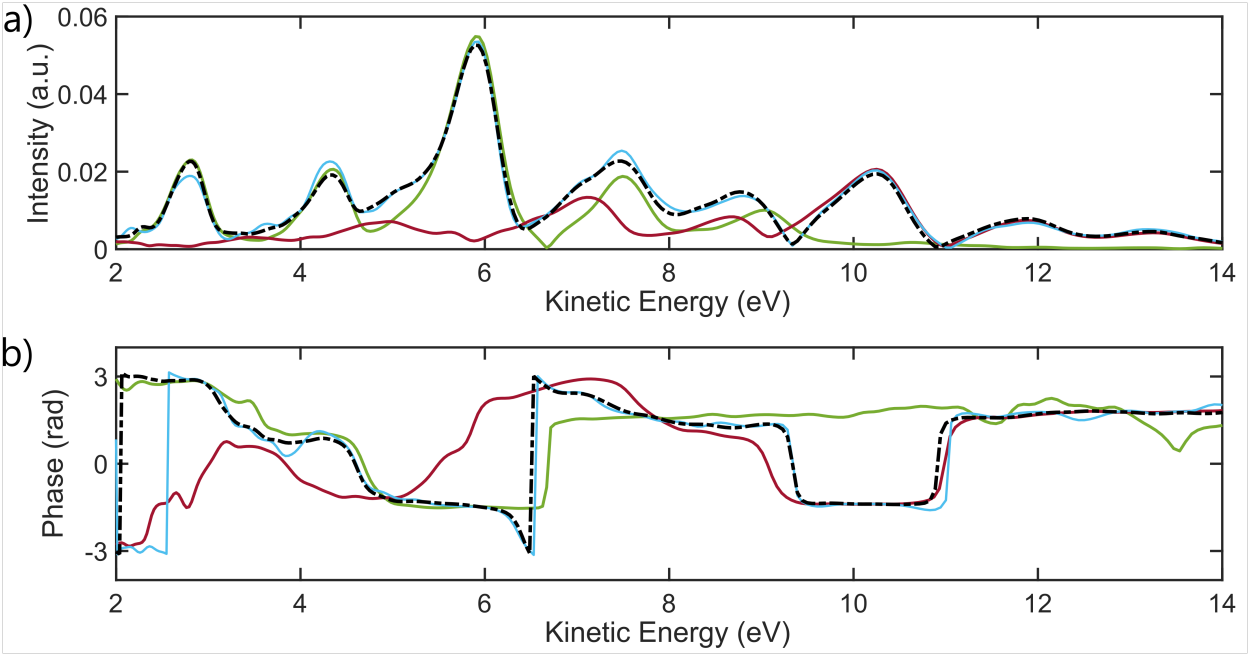


Figure 2: The (a) amplitude and (b) phase of oscillations at $2\omega_0$ for three different targets: acetylene (red curve), argon (green curve) and a mixture of both gases (blue curve). In each panel, the dashed-dotted curve denotes the reconstructed amplitude and phase for the gas-mixture obtained from the linear combination of the experimental oscillations for each of the targets, measured separately (see main text for details).

Usually, the measured phase $\phi$ consists of two contributions, $\phi = \varphi_{\mathrm{XUV}} + \varphi_{\mathrm{C_2H_2}}$. Here, the first term signifies the group delay of the broadband XUV pulse ('attochirp') and the second one corresponds to the two-photon molecular ionization. For a given APT, the $\varphi_{\mathrm{XUV}}$ is the same for two different targets.[34] The targets can be two different physical systems or, two different orbitals, ionized at the same time. For atoms, the phase $\phi$ is often measured by comparing two different orbitals of the same atom, allowing one to remove the contribution

of the attochirp by taking the difference between them.[3] For molecules, similar strategies work only in specific cases where the molecular orbitals are well-separated, so that their contributions can clearly be identified in the RABBITT spectrogram.[5,13,14] For acetylene, this is not feasible due to the strong overlap between different molecular orbitals (see Fig. 1(b)). Instead, we compare the molecular results with a well-studied atomic system, namely the argon atom, to remove the $\varphi_{\mathrm{XUV}}$-contributions. To do so, the experiment was repeated with the same harmonic comb and NIR intensities for Ar. Note that the ionization potential for Ar: 15.76 eV,[35] is higher than that of acetylene: 11.40 eV.[28] This can be seen in the amplitude of oscillations at $2\omega_0$, where the oscillations at higher kinetic energy are associated with photoelectrons coming from acetylene only (see Figure 2(a)). For Ar-only RABBITT measurements, the prominent peak at around 6 eV (green curve) corresponds to the SB14. We also extracted the phases of the oscillations at $2\omega_0$ for the different targets (see Fig. 2(b)): acetylene (red curve), argon (green curve). However, between the individual measurements of $C_2H_2$ and Ar, a long-term temporal drift of the Mach-Zehnder interferometer can affect the experimentally measured $\phi$-values. To unambiguously remove any artificial dephasing effect due to the temporal drift, we repeated the experiment with a mixture of Ar and $C_2H_2$ brought together into the interaction region of the VMI spectrometer. The amplitude and phase of oscillations at $2\omega_0$ for the mixture, extracted from the RABBITT measurements are shown as the blue curve in both Fig. 2(a) and 2(b). Using the methodology described elsewhere,[22] the individual measurements for the two targets were re-scaled in time assuming the oscillations observed in the gas-mixture to be a linear combination of those measured separately for Ar and $C_2H_2$. The reconstructed amplitude and phase of oscillations (black dashed-dotted curve in Fig. 2(a) and (b)) shows excellent agreement with those measured for the mixture, proving robustness of the technique.

Following this calibration procedure, we took the difference between the re-scaled $\phi$-values for SB14 of Ar and the contribution from the $1\pi_u$-orbital in acetylene, measured separately. It removed the contribution of the attochirp from the measurements. Since the

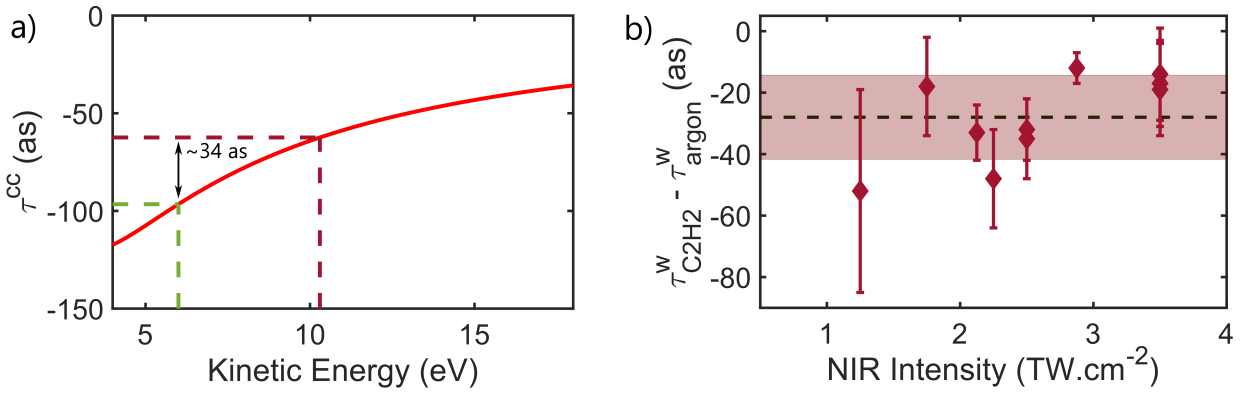


Figure 3: (a) The $\tau_{CC}$ values for SB14 for two different targets: Ar (green dashed line) and $C_2H_2$ (red dashed line). (b) The relative Wigner delay for ionization of acetylene molecule with respect to argon atom, for SB14 (photon energy: $\sim$ 21.7 eV). Each measurement represents a different intensity for the NIR dressing field. The dashed line denotes the weighted average of the measured photoionization time-delays, whereas the shaded area is the corresponding standard deviation.

measurements for $C_2H_2$ were carried out at a photon-energy region free from any autoionization, the measured two-photon molecular phase can be written as a sum of two parts,[36] $\frac{\varphi_{C_2H_2}}{2\omega_0} = \tau^{W}_{C_2H_2} + \tau^{cc}_{C_2H_2}$, where the phase $\varphi_{C_2H_2}$ has been converted into time by differentiating it with respect to the photon energy. The term $\tau^{W}_{C_2H_2}$ is the Wigner delay[37,38] for one photon ionization of the acetylene molecule and the second term is the continuum-continuum delay mediated by the NIR dressing field, inherent to the RABBITT protocol.[39,40] A similar approximation was carried out for the SB14 in Ar, which is free from the influence of the Fano resonance.[41] Combining both, the difference in RABBITT-phases, converted into a difference in time, can be expressed as, $\frac{\varphi_{C_2H_2} - \varphi_{Ar}}{2\omega_0} = \frac{\Delta\varphi}{2\omega_0} = \tau^{W}_{C_2H_2} + \tau^{cc}_{C_2H_2} - \tau^{W}_{Ar} - \tau^{cc}_{Ar}$. Because of the difference in binding energies between the two targets, the kinetic energy of the photoelectrons under consideration (i.e., for SB14) is also different. Using the long-range amplitude corrected approximation for one-electron atoms to calculate the continuum-continuum delay,[40] the difference $\tau^{cc}_{C_2H_2} - \tau^{cc}_{Ar}$ was determined to be 34 attoseconds (see Fig. 3(a)). Inserting it into the previous expression, we can therefore obtain the difference in Wigner-delay between $C_2H_2$ and Ar in terms of the difference in the $\varphi$-values as: $\tau^{W}_{C_2H_2} - \tau^{W}_{Ar} = \frac{\Delta\varphi}{2\omega_0} - 34$ as. The corresponding values of $\frac{\Delta\varphi}{2\omega_0} - 34$, for different intensities for the NIR dressing field are shown in

Fig. 3(b). Performing a weighted average over these measured values using the formula described elsewhere,[14] the difference in Wigner-delay turned out to be, $\tau^{\mathrm{W}}_{\mathrm{C_2H_2}} - \tau^{\mathrm{W}}_{\mathrm{Ar}} = -28 \pm 14$ as for the SB14, i.e., at a photon energy of approximately 21.7 eV.

## Results and Discussions

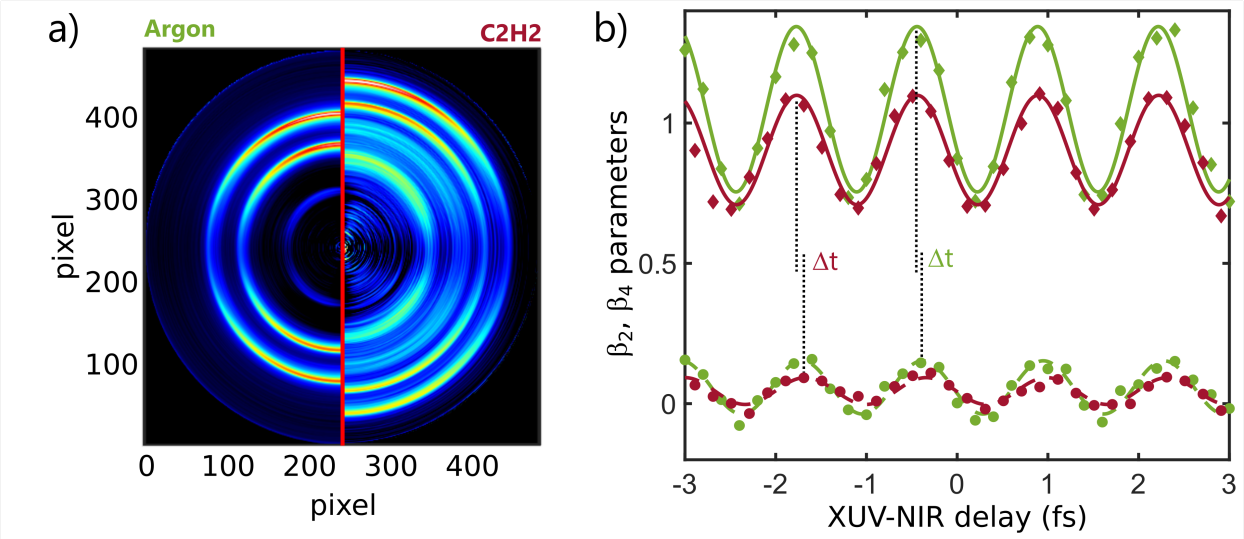


Figure 4: (a) Angle-resolved photoelectron spectra for XUV-only ionization of argon (left) and acetylene (right). (b) Time-dependent angular asymmetry parameters $\beta_2$ (diamond) and $\beta_4$ (circle) for acetylene (red) and argon (green). Note that for both systems there exists a temporal dephasing (denoted by $\Delta t$) between $\beta_2(t)$ and $\beta_4(t)$.

For SB14, the measured difference in Wigner delay implies $\tau^{\mathrm{W}}_{\mathrm{C_2H_2}} < \tau^{\mathrm{W}}_{\mathrm{Ar}}$, i.e., for ionization to a flat-continuum the photoemission from $C_2H_2$ is advanced in time compared those from Ar. To understand better the difference, we turn our attention to the angle-resolved photoelectron spectra measured for both targets using only the XUV-APT, as shown in Fig. 4(a). Compared to three distinct photoelectron channels corresponding to the ionization by three high-order harmonics 11, 13 and 15 in the case of Ar, for acetylene the spectra contain many more structures. To verify the quality of our measurement, the angular asymmetry parameter, $\beta_2$, were extracted using the well-established relation: $S(\theta) \propto S_0 [1 + \beta_2 P_2(\cos\theta)]$, where $S(\theta)$ is the angle-resolved photoelectron signal, $S_0$ denotes the total angle integrated

signal, and $P_2(\cos\theta)$ is the $2^{\text{nd}}$-order Legendre polynomial. For harmonic 13, we obtained $\beta_2^{\text{Ar}} = 0.9 \pm 0.2$, which matches quantitatively the value of 0.8 at the same photon energy ($\sim$ 20.15 eV) from synchrotron-based measurements.[42] Similarly, for harmonic 15 (photon energy: $\sim$ 23.25 eV), $\beta_2^{\text{Ar}} = 1.0 \pm 0.1$, agrees well the value of 1.0 obtained previously.[42] Evidently, the value of $\beta_2$ being close to 1 shows the $p$-character for the atomic orbital involved in valence photoionization of argon, where following single-photon ionization the most dominant contribution comes from $d$-type partial waves (Fano's propensity rule). For acetylene the valence molecular orbital is $1\pi_u$, mostly formed out of the $2p$-orbitals of the constituent carbon atoms. This particular characteristic was also noted in the branching ratios for the $X$-state of acetylene in synchrotron-based studies.[27,28] This is reflected in our measurements of the $\beta_2^{C_2H_2}$, which is equal to $0.8 \pm 0.2$ and $1.1 \pm 0.1$ for ionization by the harmonic 13 and 15, respectively. These values match well previous measurements using synchrotron radiation, which varied from 0.6 to 0.9 in this photon energy range.[27,28] Following the introduction of the NIR field, the photoelectron in the continuum can absorb or emit a NIR photon, thus requiring not just $\beta_2$, but also $\beta_4$ parameters to describe the photoelectron angular distributions. The additional $\beta_4$ parameter is usually given by, $S(\theta) \propto S_0[1 + \beta_2 P_2(\cos\theta) + \beta_4 P_4(\cos\theta)]$, where $P_4(\cos\theta)$ is the $4^{\text{th}}$-order Legendre polynomial. The extracted $\beta_2$ and $\beta_4$ values for SB14 as a function of the delay between the XUV-APT and the NIR pulse are shown in Fig. 4(b), in case of Ar and $C_2H_2$. As can be expected, for $\beta_2(t)$, the values oscillate around 1.0 for Ar and around 0.85 for $C_2H_2$, with a period of $2\omega_0$. For $\beta_4(t)$, the amplitude of oscillation is smaller for the two systems, around $\pm 0.2$. The $\beta_2(t)$ parameters for both targets were found to oscillate in phase (upper panel, Fig. 4(b)). For Ar, there exists a shift in oscillation of about 60 as between the $\beta_2(t)$ and $\beta_4(t)$ parameters. The temporal dependence of $\beta_2$ values in SB14 for argon was previously explained in terms of a generalized Fano's propensity rule, where strong asymmetry between absorption and emission pathways in the RABBITT protocol led to incomplete quantum path interference.[43] Nevertheless, no dephasing between the $\beta_2$ and $\beta_4$ parameters in argon

was reported previously at this photon energy. It clearly highlights the interplay between different partial waves in the continuum-continuum transition mediated by the NIR pulse and how its signature can be seen directly in the angular asymmetry parameters. Given that the atomic $2p$-type orbital-composition of the ionized molecular orbital in $C_2H_2$, one would also expect a similar dephasing in it. However, as shown in Fig. 4(b), the temporal shift increases to 100 as in the case of molecular $\beta_2(t)$ and $\beta_4(t)$. While it is possible to invoke the picture proposed previously in terms of the interference between different partial waves to explain this, the difference in shape between an atom and a molecule also plays an important role in this situation.

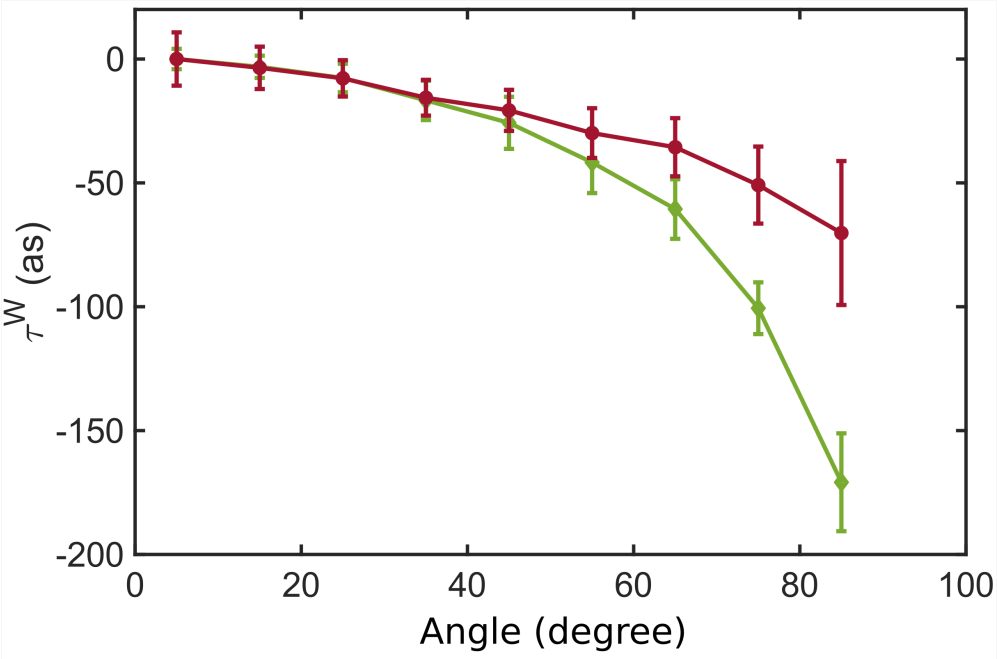


Figure 5: Angle resolved photoionization time-delay for acetylene (red circles) and argon (green diamonds). For comparison, they are normalized at 0° photoemission angle.

To highlight the difference in ionization dynamics between an atom and a linear molecule, the relative angle-dependent photoionization time delays for SB14 for both systems are shown in Fig. 5. The interferometric measurements were carried out with randomly oriented acetylene molecules in gas phase. To obtain the time-delays as a function of photoemission angle, the angle-resolved RABBITT map was integrated at 10°-angular intervals, ranging from 0°

to 90°, at each delay between the XUV-APT and the NIR pulse; an identical procedure was reported previously in case of photoionization of argon.[41] To shed light on the difference between the two systems as a function of the photoelectron emission angle, the time-delay is fixed to zero at 0° emission angle. The angular dependency of the photoionization time-delays in argon matches well previous measurements and calculations with the relative values reaching close to −100 as at around 60° emission angle.[43] Despite being emitted from a molecular orbital that is predominantly composed of atomic $2p$-orbitals, the photoelectron from acetylene does not follow this trend. Indeed, for $C_2H_2$, the photoionization time delays reach only up to −50 as near the same emission angle. This provides additional proof that for molecular photoionization the interference between different partial waves is not adequate enough to explain the angular dependency of the observed delays. As shown in the case of polycyclic aromatic hydrocarbons,[22] depending on whether the ionized system is two- or, three-dimensional, the photoionization time delay can change dramatically. It stems from the delocalization of the hole created at the instant of ionization affecting the dispersion of the emitted photoelectron wave-packet in the residual molecular potential. However, the question remains whether such a picture can be applied to even smaller systems, such as acetylene.

To provide a qualitative reasoning behind the observed trend in acetylene, first, we note that following ionization from the $1\pi_u$ orbital the molecular ion retains its linear geometry.[44] Following the same procedure applied in the case of polycyclic aromatic hydrocarbons,[22] we assume that after removal of an electron from the outermost molecular orbital, the created hole remains delocalized across the entire length of the molecule. Due to the lack of any spherical symmetry, unlike the case of atomic photoionization, the photoelectrons emitted along the C≡C bond will experience a different short-range potential compared to those emitted perpendicular to the bond. To quantify the nature of the short-range potential in these two emission directions, we calculate the electrostatic potentials using Gauss' law assuming the positively charged hole ($+e$) to be uniformly smeared out over the length ($L$)

of the molecule. The electric potential, $V_{\parallel}$, at a distance $z$ from one end of the molecule along the C≡C bond is given by, $V_{\parallel} = \frac{e}{4\pi\varepsilon_0 L}\ln\left(1+\frac{L}{z}\right)$. Here, $\varepsilon_0$ is the permittivity of free-space. Similarly, at an arbitrary point perpendicular to the C≡C bond, the electric potential $V_{\perp}$ can be written as, $V_{\perp} = \frac{2e}{4\pi\varepsilon_0 L}\ln\left(\frac{L}{2x}+\sqrt{1+\frac{L^2}{4x^2}}\right)$, where $x$ is the distance of the point from the center of mass of the molecule. Thus, the potential energy of the photoelectron in these two directions can be written as, $\Phi_{\parallel} = -eV_{\parallel}$ and $\Phi_{\perp} = -eV_{\perp}$. For $z > L$ and $x > L$, the Taylor-series expansion yields that, $\Phi_{\parallel} = -\frac{e^2}{4\pi\varepsilon_0 L}\left[\frac{L}{z} - \frac{1}{2}\frac{L^2}{z^2} + \mathcal{O}\left(\frac{L^3}{z^3}\right)\right]$ and $\Phi_{\perp} = -\frac{e^2}{4\pi\varepsilon_0 L}\left[\frac{L}{x} - \frac{1}{24}\frac{L^3}{x^3} + \mathcal{O}\left(\frac{L^5}{x^5}\right)\right]$. While the first term in both cases represent the long-range Coulomb potential, the second term representing the short-range potential (since it falls faster than the first term) is different.

For the potential energy $\Phi_{\parallel}^{\text{short}} = \frac{e^2 L}{8\pi\varepsilon_0}\frac{1}{z^2}$, the scattering phase-shift is constant, i.e., independent of kinetic energy of the electron, because the potential is scale-invariant. It implies that the solution of the static Schródinger equation for the scattering states can only be a function of $pz$, since the Hamiltonian does not change its form under the transformations, $t \to \mu t$, $z(t) \to z(\mu t)/\sqrt{\mu}$, and $p(t) \to p(\mu t)\sqrt{\mu}$, where $p$ is the momentum and $\mu$ is a dimensionless factor.[45] Since the existence of an energy dependent phase will be incompatible with this symmetry, the scattering phase itself becomes energy independent. Thus, the Wigner delay calculated by taking the derivative of the scattering phase with respect to the kinetic energy of the photoelectron is zero. To obtain a measure of the 'time-delay' associated with this potential we can assume the photoelectron with kinetic energy $E \sim 10$ eV to be trapped by the $1/z^2$ repulsive barrier, much like in the case of a shape resonance.[14] The potential energy can be re-written as, $\Phi_{\parallel}^{\text{short}}(z) = -\Phi_0$ (equal to the binding energy of the electron) for $z \leq z_0$ and $\Phi_{\parallel}^{\text{short}}(z) = \alpha/z^2$ for $z > z_0$, where $\alpha = \frac{e^2 L}{8\pi\varepsilon_0}$. Using the Wentzel-Krammers-Brillouin (WKB) approximation,[46] the probability for tunneling can be expressed as, $\rho \sim \exp\left[-\frac{2}{\hbar}\int_{z_0}^{z_1}\left|\sqrt{2m_e\left(\frac{\alpha}{z^2}-E\right)}\right|dz\right]$, where $z_0 < z_1$ and $m_e$ is the mass of the electron. The photoelectron can collide back and forth with the 'wall' at $z_0$. The time between successive collisions is given by, $2z_0/v$, where $v$ is the velocity of the electron. The

probability for escaping per unit time is $\rho v/2z_0$. The trapping time or, the time delay in the presence of this barrier can therefore be written approximately as, $\tau_{\parallel} \approx 2z_0/v\,(\rho^{-1}-1)$. To evaluate $\rho$, we assume $z_0 \sim L = 3.324$ Å, which includes the length of the two C−H bonds and the C≡C bond in its neutral ground state.[44] Following ionization of the $1\pi_u$ orbital, the total length of $C_2H_2^+$ ion in the the $X$-state is increased by 1.34%, resulting in $z_1 = 3.37$ Å.[44] With this, we obtain $\rho \approx 0.88$ and thus, the associated time-delay, $\tau_{\parallel} \approx 48$ as.

Now, for the potential energy $\Phi_{\perp}^{\text{short}} = \frac{e^2L^2}{96\pi\varepsilon_0}\frac{1}{x^3}$, the Hamiltonian does not have the scale invariance as described above. It leads to an energy dependent phase and hence, we can use the usual definition of the Wigner delay. The asymptotic form of the scattering phase $\delta$ at $x \to +\infty$ can be obtained from the first order Born approximation as, $\tan\delta \approx -\frac{2m_e\gamma}{\hbar^2 k}\int_0^{\infty}\cos^2(kx)\,\frac{dx}{x^3}$, where $\gamma = \frac{e^2L^2}{96\pi\varepsilon_0}$ and $k$ is the wave-vector.[47–49] Because the potential itself diverges at $x = 0$, this integral diverges as well. A regularization of the potential leads to: $\Phi_{\perp}^{\text{short}} = \infty$ for $x \le x_0$ and $\Phi_{\perp}^{\text{short}} = \gamma/x^3$ for $x > x_0$. In this situation, the phase can be rewritten as, $\delta \approx -\frac{2m_e\gamma k}{\hbar^2}\int_{kx_0}^{\infty}\cos^2(x')\,\frac{dx'}{x'^3}$. Note that the phase shift depends on the wave-vector, and hence, on the kinetic energy of the electron. To obtain the correct order of magnitude of the phase-shift for a given value of $k$, we assume that it is always possible to find a value of $x_0$, for which the *maximum* value of the integral is 1. With this approximation a simplified expression of the phase-shift, $\delta \approx -\frac{2m_e\gamma k}{\hbar^2}$ is found. After taking the derivative of $\delta$ with respect to the electron kinetic energy, and inserting the values of the parameters we get $\tau_{\perp} \approx -92$ as at $E = 10$ eV.

Evidently, depending on whether the photoelectron from acetylene is emitted along or perpendicular to the molecular symmetry axis (C≡C bond), it can be either 'delayed' or 'advanced' in time, compared to a free electron. In particular, for an electron emitted at an intermediate angle, such as 45° or, 60° as opposed to 0° or, 90°, it will experience a mixture of two different short-range potential, altering the photoionization time-delays. The total photoionization time-delay for the randomly oriented molecule can approximately be obtained by performing a weighted average of the time-delays in the parallel and perpendicular directions

with respect to the corresponding ionization cross-sections: $\tau_{\text{total}} = \left(\frac{2}{3}\sigma_{\perp}\tau_{\perp} + \frac{1}{3}\sigma_{\parallel}\tau_{\parallel}\right)/\sigma_{\text{total}}$. Here, $\sigma_{\perp}$ ($\sigma_{\parallel}$) denotes the photoionization cross-sections when the polarization axis of the ionizing light-pulse is perpendicular (parallel) to the molecular symmetry axis. At photon energy of 21.5 eV, the experimentally measured total ionization cross-section for the X-state in acetylene, $\sigma_{\text{total}} \approx 14.36$ Mb.[50] To estimate $\sigma_{\perp}$ and $\sigma_{\parallel}$ for ionization of the $1\pi_u$ orbital, we can use the theoretical cross-sections to reach the $\delta_g$ and $\sigma_g$ continua, respectively.From the results based on TD-DFT calculations provided elsewhere, the values were extrapolated to be $\sigma_{\perp} \approx 10.33$ Mb and $\sigma_{\parallel} \approx 1.67$ Mb at the same photon energy.[30] Plugging in all the numbers, the time-delay turns out to be, $\tau_{\text{total}} \approx -42$ as. This agrees qualitatively with the observed time-delay-difference between acetylene and argon, $\tau^{\text{W}}_{\text{C}_2\text{H}_2} - \tau^{\text{W}}_{\text{Ar}} = -28 \pm 14$ as, which arises mainly due to the molecular short-range potential. It implies that the photoionization dynamics of the outer-valence orbital in acetylene away from the threshold is dominated by the short-range potential perpendicular to molecular symmetry axis. Compared to atoms, where only the interference between different partial waves plays a role, time-delays for molecular ionization carry the signature of the non-spherical symmetry of the hole created at the instant of photoionization, which can lead to an advance in the photoionization time, as observed here. Using an angle-resolved RABBITT spectrogram in combination with a semi-classical derivation, we could efficiently identify its relevance even in the case of a relatively small linear molecule such as, acetylene.

# Conclusions

In summary, we have shown that photoionization time delays can be a sensitive tool for understanding the delocalization of the hole following sudden removal of an electron from a molecular orbital. While for atomic photoionization, it is the interference between several partial waves leading to the same final state in the ionization continuum, for molecular photoionization in addition to such interference one needs to account for the shape of the

molecule itself. We showcase this concept using a tetra-atomic linear hydrocarbon molecule. With the onset of applications of the RABBITT technique to more and more complex systems in recent times, we believe our results will inspire additional studies, both experimental and theoretical, to properly account for these effects stemming from the shape of the molecular potentials in the associated photoionization time-delays.

# Author Information

## Corresponding Authors

*(S.N.) E-mail: saikat.nandi@univ-lyon1.fr.

*(F.L.) E-mail: franck.lepine@univ-lyon1.fr.

## Author Contributions

All authors contributed significantly towards the realization of the project.

## Notes

The authors declare no competing financial interest.

# Acknowledgement

We thank CNRS, Fédération de Recherche André Marie Ampère (FRAMA), Agence Nationale de la Recherche (ANR Circé, ANR-16-CE30-0012) and COST ATTOCHEM for financial support.

# References


(1) Schultze, M.; Fiess, M.; Karpowicz, N.; Gagnon, J.; Korbman, M.; Hofstetter, M.; Neppl, S.; Cavalieri, A. L.; Komninos, Y.; Mercouris, Th., et al. Delay in photoemission. *Science* **2010**, *328*, 1658-1662.

(2) Klünder, K.; Dahlström, J. M.; Gisselbrecht, M.; Fordell, T.; Swoboda, M.; Guénot, D.; Johnsson, P.; Caillat, J.; Mauritsson, J.; Maquet, A., et al. Probing single-photon ionization on the attosecond time scale. *Phys. Rev. Lett.* **2011**, *106*, 143002.

(3) Isinger, M.; Squibb, R. J.; Busto, D.; Zhong, S.; Harth, A.; Kroon, D.; Nandi, S.; Arnold, C. L.; Miranda, M.; Dahlström, J. M., et al. Photoemission in the time and frequency domain. *Science* **2017**, *358*, 893-896.

(4) Haessler, S.; Fabre, B.; Higuet, J.; Caillat, J.; Ruchon, T.; Breger, P.; Carré, B.; Constant, E.; Maquet, A.; Mével, E., et al. Phase-resolved attosecond near-threshold photoionization of molecular nitrogen. *Phys. Rev. A* **2009**, *80*, 011404(R).

(5) Huppert, M.; Jordan, I.; Baykusheva, D.; von Conta, A.; Wörner, H. J. Attosecond Delays in Molecular Photoionization. *Phys. Rev. Lett.* **2016**, *117*, 093001.

(6) Cattaneo, L.; Vos, J.; Bello, R. Y.; Palacios, A.; Heuser, S.; Pedrelli, L.; Lucchini, M.; Cirelli, C.; Martín, F.; Keller, U. Attosecond coupled electron and nuclear dynamics in dissociative ionization of $H_2$. *Nat. Phys.* **2018**, *14*, 733-738.

(7) Vos, J.; Cattaneo, L.; Patchkovskii, S.; Zimmermann, T.; Cirelli, C.; Lucchini, M.; Kheifets, A.; Landsman, A. S.; Keller, U. Orientation-dependent stereo Wigner time delay and electron localization in a small molecule. *Science* **2018**, *360*, 1326-1330.

(8) Tao, Z.; Chen, C.; Szilvási, T.; Keller, M.; Mavrikakis, M.; Kapteyn, H.; Murnane, M. Direct time-domain observation of attosecond final-state lifetimes in photoemission from solids. *Science* **2016**, *353*, 62-67.

(9) Ossiander, M.; Riemensberger, J.; Neppl, S.; Mittermair, M.; Schäffer, M.; Duensing, A.; Wagner, M. S.; Heider, R.; Wurzer, M.; Gerl, M., et al. Absolute timing of the photoelectric effect. *Nature* **2018**, *561*, 374–377.

(10) Jordan, I.; Huppert, M.; Rattenbacher, D.; Peper, M.; Jelovina, D.; Perry, C.; von Conta, A.; Schild, A.; Wörner, H. J. Attosecond spectroscopy of liquid water. *Science* **2020**, *369*, 974-979.

(11) Kotur, M.; Guénot, D.; Jiménez-Galán, Á.; Kroon, D.; Larsen, E. W.; Louisy, M.; Bengtsson, S.; Miranda, M.; Mauritsson, J.; Arnold, C. L., et al. Spectral phase measurement of a Fano resonance using tunable attosecond pulses. *Nat. Comm.* **2016**, *7*, 10566.

(12) Gruson, V.; Barreau, L.; Jiménez-Galan, Á.; Risoud, F.; Caillat, J.; Maquet, A.; Carré, B.; Lepetit, F.; Hergott, J.-F.; Ruchon, T., et al. Attosecond dynamics through a Fano resonance: Monitoring the birth of a photoelectron. *Science* **2016**, *354*, 734-738.

(13) Loriot, V.; Marciniak, A.; Nandi, S.; Karras, G.; Hervé, M.; Constant, E.; Plésiat, E.; Palacios, A.; Martín, F.; Lépine, F. High harmonic generation-2$\omega$ attosecond stereo-photoionization interferometry in $N_2$. *J. Phys. Photonics* **2020**, *2*, 024003.

(14) Nandi, S.; Plésiat, E.; Zhong, S.; Palacios, A.; Busto, D.; Isinger, M.; Neoričić, L.; Arnold, C. L.; Squibb, R. J.; Feifel, R., et al. Attosecond timing of electron emission from a molecular shape resonance. *Sci Adv.* **2020**, *6*, aba7762.

(15) Holzmeier, F.; Joseph, J.; Houver, J. C.; Lebech, M.; Dowek, D.; Lucchese, R. R. Influence of shape resonances on the angular dependence of molecular photoionization delays. *Nat. Comm.* **2021**, *12*, 7343.

(16) Gong, X.; Jiang, W.; Tong, J.; Qiang, J.; Lu, P.; Ni, H.; Lucchese, R.; Ueda, K.; Wu,

J. Asymmetric attosecond photoionization in molecular shape resonance. *Phys. Rev. X* **2022**, *12*, 011002.

(17) Beaulieu, S.; Comby, A.; Clergerie, A.; Caillat, J.; Descamps, D.; Dudovich, N.; Fabre, B.; Géneaux, R.; Légaré, F.; Petit, S., et al. Attosecond-resolved photoionization of chiral molecules. *Science* **2017**, *358*, 1288-1294.

(18) Barillot, T.; Cauchy, C.; Hervieux, P.-A.; Gisselbrecht, M.; Canton, S. E.; Johnsson, P.; Laksman, J.; Mansson, E. P.; Dahlström, J. M.; Magrakvelidze, M., et al. Angular asymmetry and attosecond time delay from the giant plasmon resonance in $C_60$ photoionization. *Phys. Rev. A* **2015**, *91*, 033413.

(19) Biswas, S.; Benjamin, F.; Ortmann, L.; Schötz, J.; Schweinberger, W.; Zimmermann, T.; Pi, L.; Baykusheva, D.; Masood, H. A.; Liontos, I., et al. Probing molecular environment through photoemission delays. *Nat. Phys.* **2020**, *16*, 778–783.

(20) Ahmadi, H.; Plésiat, E.; Moioli, M.; Frassetto, F.; Poletto, L.; Decleva, P.; Schröter, C. D.; Pfeifer, T.; Moshammer, R.; Palacios, A., et al. Attosecond photoionisation time delays reveal the anisotropy of the molecular potential in the recoil frame. *Nat. Comm.* **2022**, *13*, 1242.

(21) Gong, X.; Heck, S.; Jelovina, D.; Perry, C.; Zinchenko, K.; Lucchese, R.; Wörner, H. J. Attosecond spectroscopy of size-resolved water clusters. *Nature* **2022**, *609*, 507–511.

(22) Loriot, V.; Boyer, A.; Nandi, A.; Plésiat, E.; Marciniak, A.; Garcia, C.; Lara-Astiaso, M.; Palacios, A.; Decleva, P.; Martín, F.; Lépine, F. Attosecond metrology of 2D charge distribution in molecules. arXiv:2209.02445 (physics.chem-ph), submitted 6 Sep 2022, DOI: https://doi.org/10.48550/arXiv.2209.02445.

(23) Gong, X.; Plésiat, E.; Palacios, A.; Heck, S.; Martín, F.; Wörner, H. J. Attosecond delays between dissociative and non-dissociative ionization of polyatomic molecules. *Nat. Comm.* **2023**, *14*, 4402.

(24) Ertel, D.; Busto, D.; Makos, I.; Schmoll, M.; Benda, J.; Ahmadi, H.; Moioli, M.; Frassetto, F.; Poletto, L.; Schröter, C. D., et al. Influence of nuclear dynamics on molecular attosecond photoelectron interferometry. *Sci. Adv.* **2023**, *9*, adh7747.

(25) Paul, P. M.; Toma, E. S.; Breger, P.; Mullot, G.; Augé, F.; Balcou, Ph.; Muller, H. G.; Agostini, P. Observation of a train of attosecond pulses from high harmonic generation. *Science* **2001**, *292*, 1689-1692.

(26) Boyer. A.; Nandi, S.; Loriot, V. Attosecond probing of photoionization dynamics from diatomic to many-atom molecules. *Eur. Phys. J. Sp. T.* **2023**, *232*, 2001-2009.

(27) Holland, D.M.P.; MacDonald, M.A.; Hayes, M.A.; Karlsson, L.; Wannberg. B.; A photoelectron spectroscopy study of the valence shell photoionization dynamics of acetylene. *J. Elec. Spec. Rel. Phenom.* **1998**, *97*, 253–263.

(28) Holland, D.M.P.; MacDonald, M.A.; Hayes, M.A.; Karlsson, L.; Wannberg. B.; A photoelectron spectroscopy study of the valence shell photoionization dynamics of acetylene. *J. Elec. Spec. Rel. Phenom.* **1999**, *104*, 245–255.

(29) Lynch, D.; Lee, M.T.; Lucchese, R. R.; McKoy, V. Studies of the photoionization cross sections of acetylene. *J. Chem. Phys.* **1984**, *80*, 1907.

(30) Fronzoni, G.; Stener, M.; Decleva, P. Valence and core photoionization dynamics of acetylene by TD-DFT continuum approach. *Chem. Phys.* **2004**, *298*, 141-153.

(31) Marciniak, A.; Despré, V.; Loriot, V.; Karras, G.; Hervé, M.; Quintard, L.; Catoire, F.; Joblin, C.; Constant, E.; Kuleff, A. I., et al. Electron correlation driven non-adiabatic relaxation in molecules excited by an ultrashort extreme ultraviolet pulse. *Nat. Comm.* **2019**, *10*, 337.

(32) Hervé, M.; Despré, V.; Castellanos Nash, P.; Loriot, V.; Boyer, A.; Scognamiglio, A.; Karras, G.; Brédy, R.; Constant, E.; Tielens, A.G.G.M., et al. Ultrafast dynamics

of correlation bands following XUV molecular photoionization. *Nat. Phys*, **2021**, *17*, 327-331.

(33) Loriot, V.; Marciniak, A.; Quintard, L.; Despré, V.; Schindler, B.; Compagnon, I.; Concina, B.; Celep, G.; Bordas, C.; Catoire, F., et al. Resolving XUV induced femtosecond and attosecond dynamics in polyatomic molecules with a compact attosecond beamline. *J. Phys.: Conf. Ser.* **2015**, *635*, 012006.

(34) Mairesse, Y.; de Bohan, A.; Frasinski, L. J.; Merdji, H.; Dinu, L. C.; Monchicourt, P.; Breger, P.; Kovačev, M.; Taïeb, R.; Carré, B., et al. Attosecond synchronization of high-harmonic soft x-rays. *Science* **2003**, *302*, 1540-1543.

(35) Kramida, A., Ralchenko, Y., Reader, J. and NIST ASD Team (2022), NIST Atomic Spectra Database (ver. 5.10). National Institute of Standards and Technology, Gaithersburg, MD.

(36) Baykusheva, D.; Wörner, H. J. Theory of attosecond delays in molecular photoionization. *J. Chem. Phys.* **2017**, *146*, 124306.

(37) Wigner, E. P. Lower limit for the energy derivative of the scattering phase shift. *Phys. Rev.* **1955**, *98*, 145-147.

(38) Smith, F. T. Lifetime matrix in collision theory. *Phys. Rev.* **1960**, *118*, 349-356.

(39) Dahlström, J. M.; Guénot, D.; Klünder, K.; Gisselbrecht, M.; Mauritsson, J.; L'Huillier, A.; Maquet, A.; Taïeb, R. Theory of attosecond delays in laser-assisted photoionization. *Chem. Phys.* **2011**, *414*, 53-64.

(40) Dahlström, J. M.; L'Huillier, A.; Maquet, A. Introduction to attosecond delays in photoionization. *J. Phys. B: At. Mol. Opt. Phys.* **2012**, *45*, 183001.

(41) Cirelli, C.; Marante, C.; Heuser, S.; Petersson, C. L. M.; Jiménez Galán, Á.; Argenti,

L.; Zhong, S.; Busto, D.; Isinger, M.; Nandi, S., et al. Anisotropic photoemission time delays close to a Fano resonance. *Nat. Comm.* **2018**, *9*, 955.

(42) Southworth, S.; Parr, A.; Hardis, J.; Dehmer, J.; Holland, D. Calibration of a monochromator / spectrometer system for the measurement of photoelectron angular distributions and branching ratios. *Nucl. Instr. Meth Phys. Res A* **1986**, *246*, 782–786.

(43) Busto, D.; Vinbladh, J.; Zhong, S.; Isinger, M.; Nandi, S.; Maclot, S.; Johnsson, P.; Gisselbrecht, M.; L'Huillier, A.; Lindroth, E., et al. Fano's Propensity Rule in Angle-Resolved Attosecond Pump-Probe Photoionization. *Phys. Rev. Lett.* **2019**, *123*, 133201.

(44) Chau, F. T. Ionic geometries of acetylene in the $X^2\Pi_u$, and $B^2\Sigma_u^+$ ionic states. *Chem. Phys. Lett.* **1990**, *169*, 43-48.

(45) Jackiw, R. Introducing scale symmetry. *Phys. Today* **1972**, *25*, 23-27.

(46) Landau, L.D.; Lifshitz, E.M. Quantum Mechanics (Non-Relativistic Theory). **1977**, 3rd Edition, Pergamon Press, Oxford.

(47) Kahn A. H. Phase-Shift Method for One-Dimensional Scattering. *Am. J. Phys.* **1961**, *29*, 77.

(48) Eberly, J. H. Quantum Scattering Theory in One Dimension. *Am. J. Phys.* **1965**, *33*, 771–773.

(49) Formánek, J. On phase shift analysis of one-dimensional scattering. *Am. J. Phys.* **1976**, *44*, 778–779.

(50) Cooper, G.; Ibuki, T.; Iida, Y.; Brion, C. E. Absolute dipole oscillator strengths for photoabsorption and the molecular and dissociative photoionization of acetylene. *Chem. Phys.* **1988**, *125*, 307-320.